Supporting Information for "A stochastic view of the 2020 Elazığ M_w6.8 earthquake (Turkey)"

Théa Ragon[1], Mark Simons[1], Quentin Bletery[2], Olivier Cavalié[2], Eric Fielding[3]

[1]Seismological Laboratory, California Institute of Technology, Pasadena, CA, USA.

[2]Université Côte dAzur, IRD, CNRS, Observatoire de la Côte dAzur, Géoazur, France.

[3]Jet Propulsion Laboratory, California Institute of Technology, Pasadena, CA, USA.

Contents of this file

1. Tables S1 to S3
2. Figures S1 to S15

0094-8276/20/$5.00

Width (km)	ρ **(mg/m^3)**	**Vp (km/s)**	**Vs (km/s)**	μ **(GPa)**	Std in μ
3.0	2.20	3.5	2.33	11.9	6
2.0	2.20	5.0	3.33	24.4	5
4.0	2.65	6.0	4.00	42.4	3.5
26.0	2.85	6.5	4.33	53.4	3
0.0	5.85	7.8	5.20	77.4	3

Table S1. Assumed elastic structure and assumed uncertainties (std = standard deviation). Poisson's ratio is assumed constant for each layer.

Satellite	**Orbital direction**	**Track**	**Interferogram pair**
ALOS 2	ascending	A182	2020/01/03 - 2020/01/31
ALOS 2	descending	D077	2019/03/03 - 2020/03/01
Sentinel 1A	ascending	TA116	2020/01/21 - 2020/01/27
Sentinel 1A	descending	TD123	2020/01/22 - 2020/01/28

Table S2. Interferometric pairs used for the study of the Elazig earthquake.

Data	**RMS for preferred model**	**RMS for simple model**
ALOS 2 asc. A182	2.2200	3.4677
ALOS 2 dsc. D077	6.3968	5.6185
PO ALOS 2 asc. A182	8.1091	7.4120
PO ALOS 2 dsc. D077	7.4905	7.3474
Sentinel 1A asc. TA116	2.0717	2.0475
Sentinel 1A dsc. TD123	4.4579	3.2895
GPS	0.9466	0.7139

Table S3. Residuals (root mean square) between predictions and observations for our preferred model (complex fault geometry, accounting for uncertainties) and the simple model (planar geometry, neglecting epistemic uncertainties).

References

Bletery, Q., Cavalié, O., Nocquet, J.-M., & Ragon, T. (2020). Distribution of Interseismic Coupling Along the North and East Anatolian Faults Inferred From InSAR and GPS Data. *Geophysical Research Letters*, *47*(16), e2020GL087775. doi: 10.1029/2020GL087775

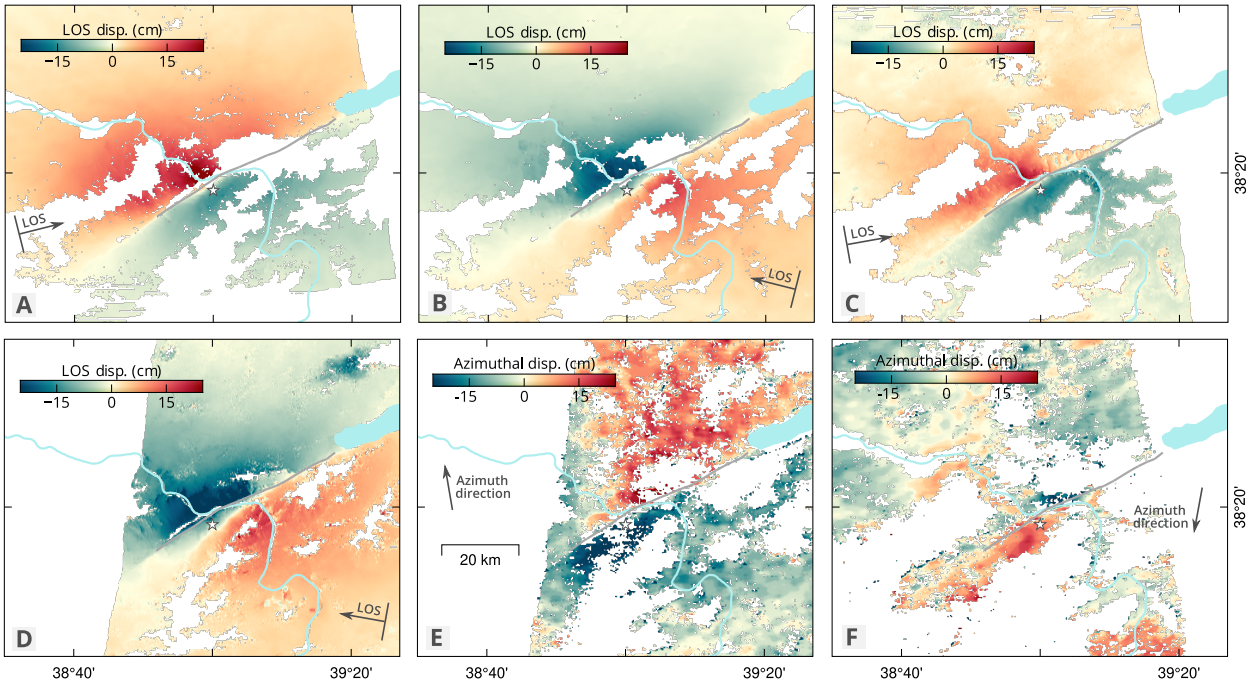

Figure S1. Observations used in thus study. (a) Surface displacement in the satellite line-of-sight (LOS) direction from a Sentinel-1 ascending interferogram (01/21/2020-01/27/2020). (b) Surface displacement from a Sentinel-1 descending interferogram (01/22/2020-01/28/2020). (c) Surface displacement from an ALOS-2 ascending interferogram (01/03/2020-01/31/2020). (d) Surface displacement from an ALOS-2 descending interferogram (03/03/2019-03/01/2020). (e) Pixel-offset surface displacement in the satellite along-track (azimuth) direction from the ALOS-2 descending pair (03/03/2019-03/01/2020). (f) Pixel-offset surface displacement in the satellite azimuth direction from the ALOS-2 ascending pair (01/03/2020-01/31/2020). The surface projection of the satellite LOS direction is positive in the ground-to-satellite direction.

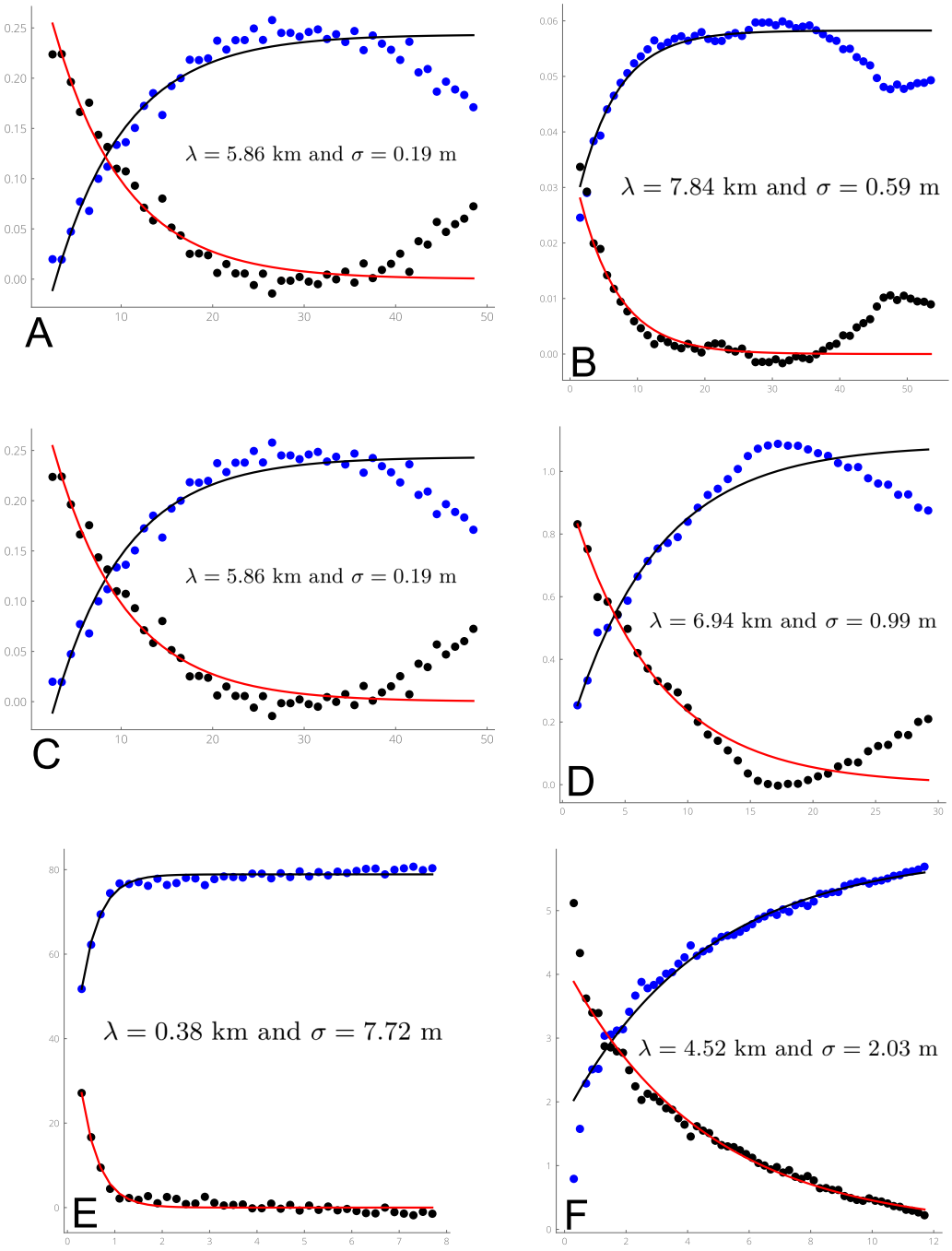

Figure S2. Empirical covariance functions (cm^2) in fonction of the distance between data points (km) for the pairs used in the study of the Elazig earthquake. Covariances have been calculated neglecting the deformation located within $[38.4, 39.4]$ in longitude and $[38.15, 38.5]$ in latitude. A) Sentinel 1 Ascending. B) Sentinel 1 Descending. C) ALOS2 ascending. D) ALOS2 descending. E) ALOS2 descending pixel-offset. F) ALOS2 ascending pixel-offset. Radially symmetric empirical covariance functions (black points) and associated best fit exponential functions (red curve), as well as semivariograms (black curve) are shown. For each interferogram, we compute the empirical covariance as a function of the inter-pixel distance and then fit an exponential function (Jolivet et al. 2012) such that σ and λ characterize $C(i,j) = \sigma^2 e^{-\frac{||i,j||^2}{\lambda}}$.

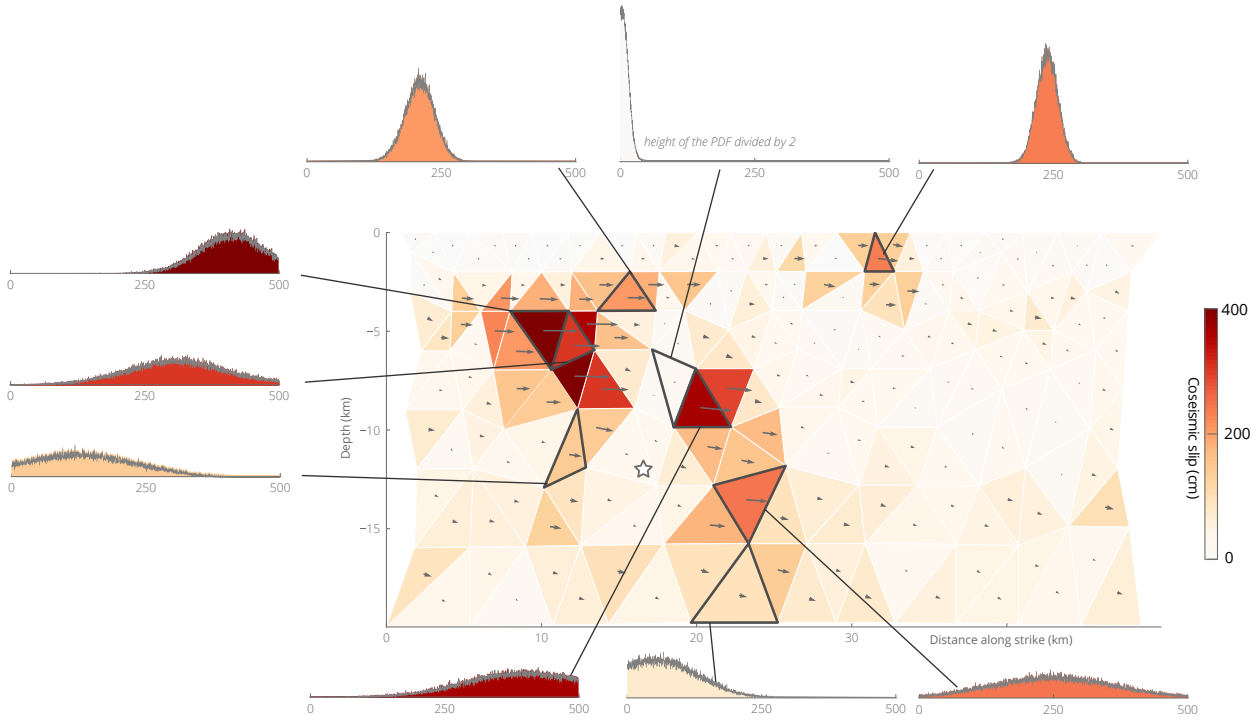

Figure S3. Posterior marginal probability density functions for selected strike-slip parameters of our preferred slip model.

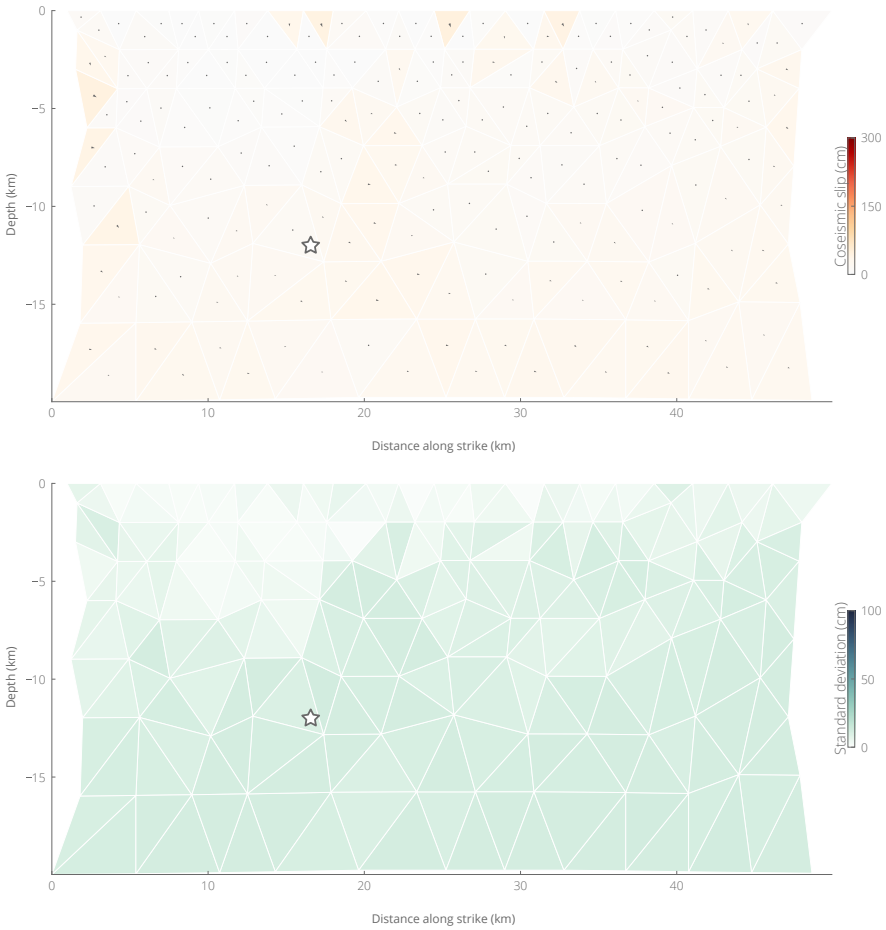

Figure S4. Inferred dip-slip amplitude (top) and associated standard deviation (bottom) for our preferred slip model.

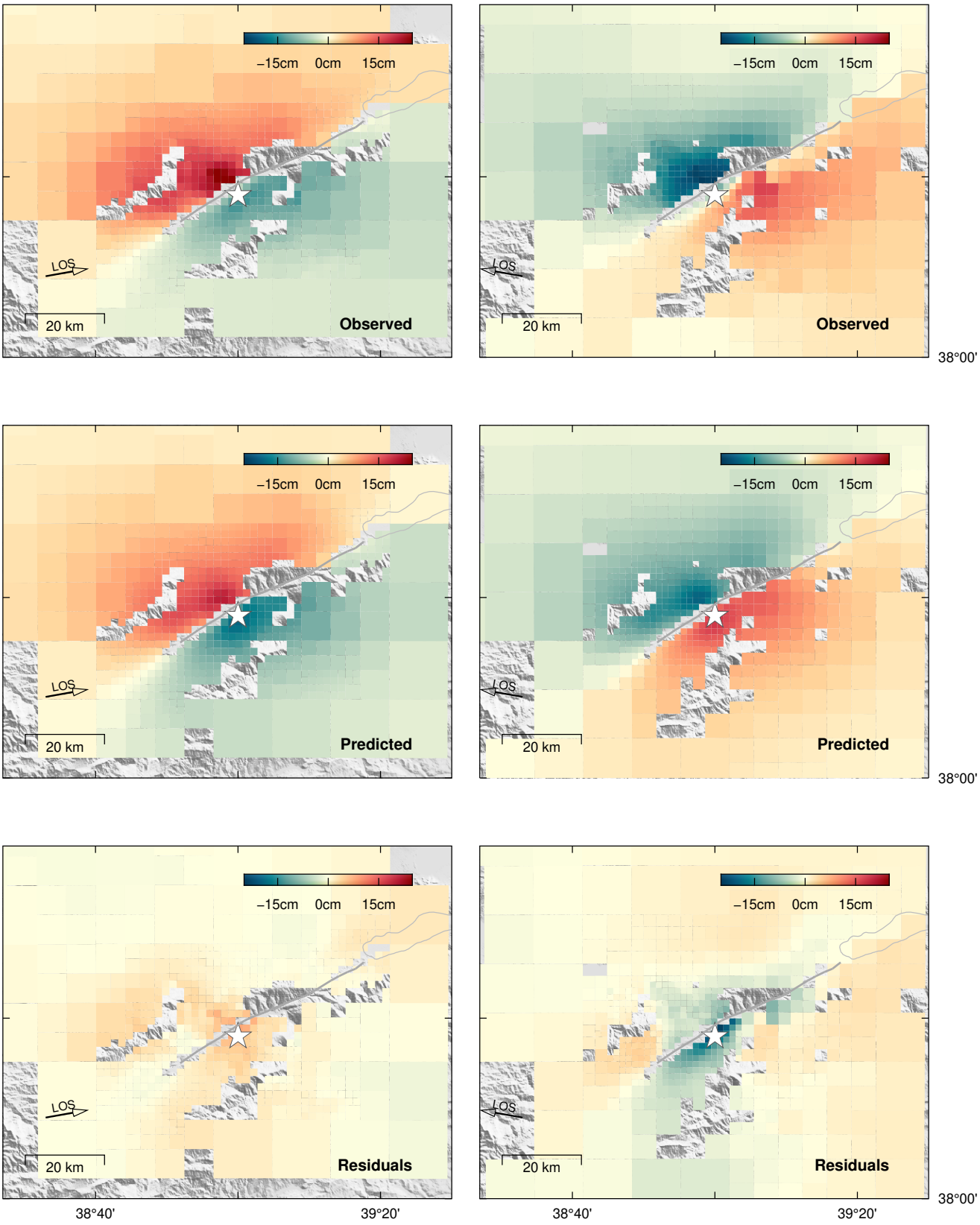

Figure S5. Observed and predicted surface displacement in the LOS direction for the Sentinel-1 ascending (left) and descending (right) interferograms. Predictions are inferred from the average model. The assumed fault trace is shown with a dark gray line.

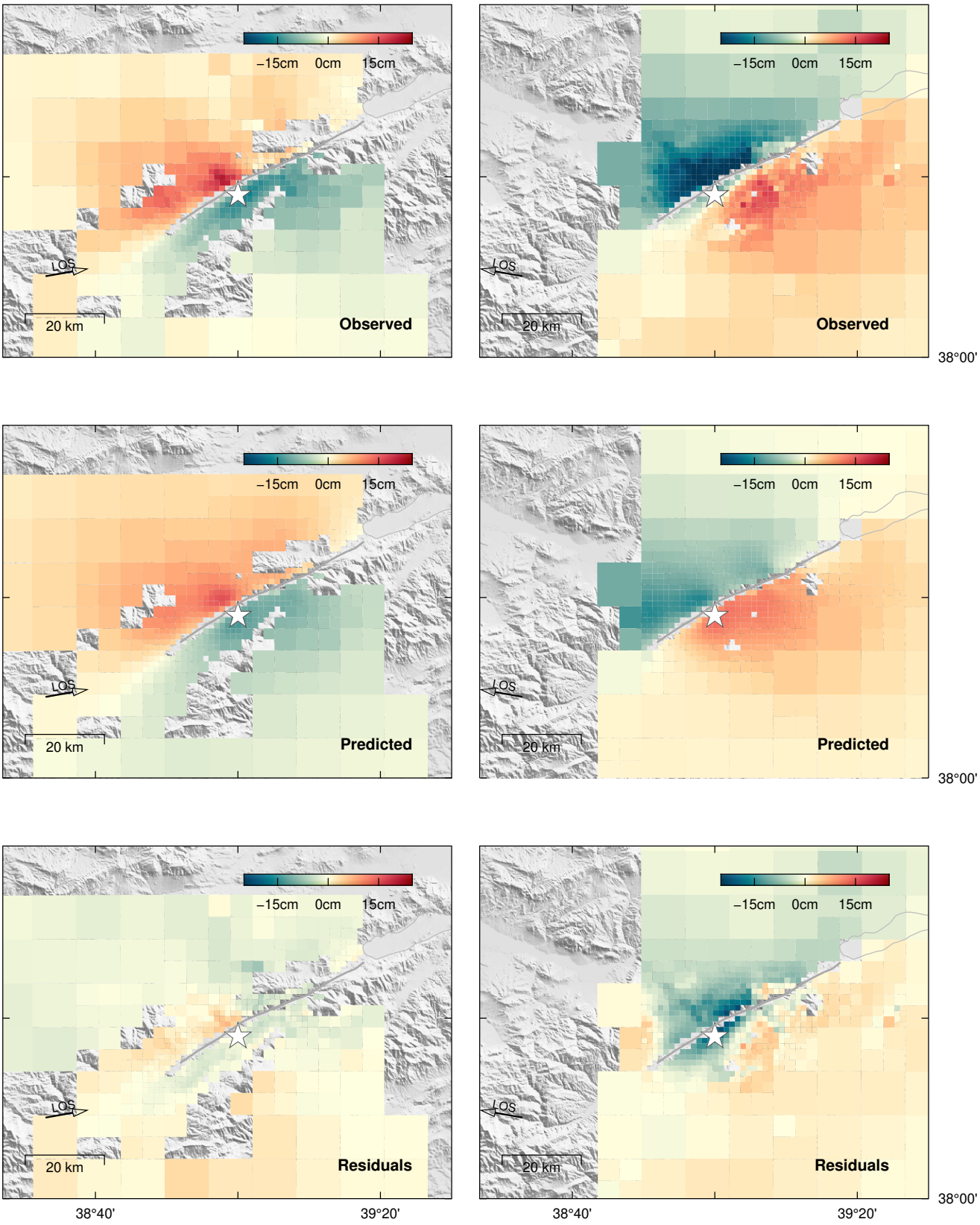

Figure S6. Observed and predicted surface displacement in the LOS direction for the ALOS 2 ascending (left) and descending (right) interferograms. Predictions are inferred from the average model. The assumed fault trace is shown with a dark gray line.

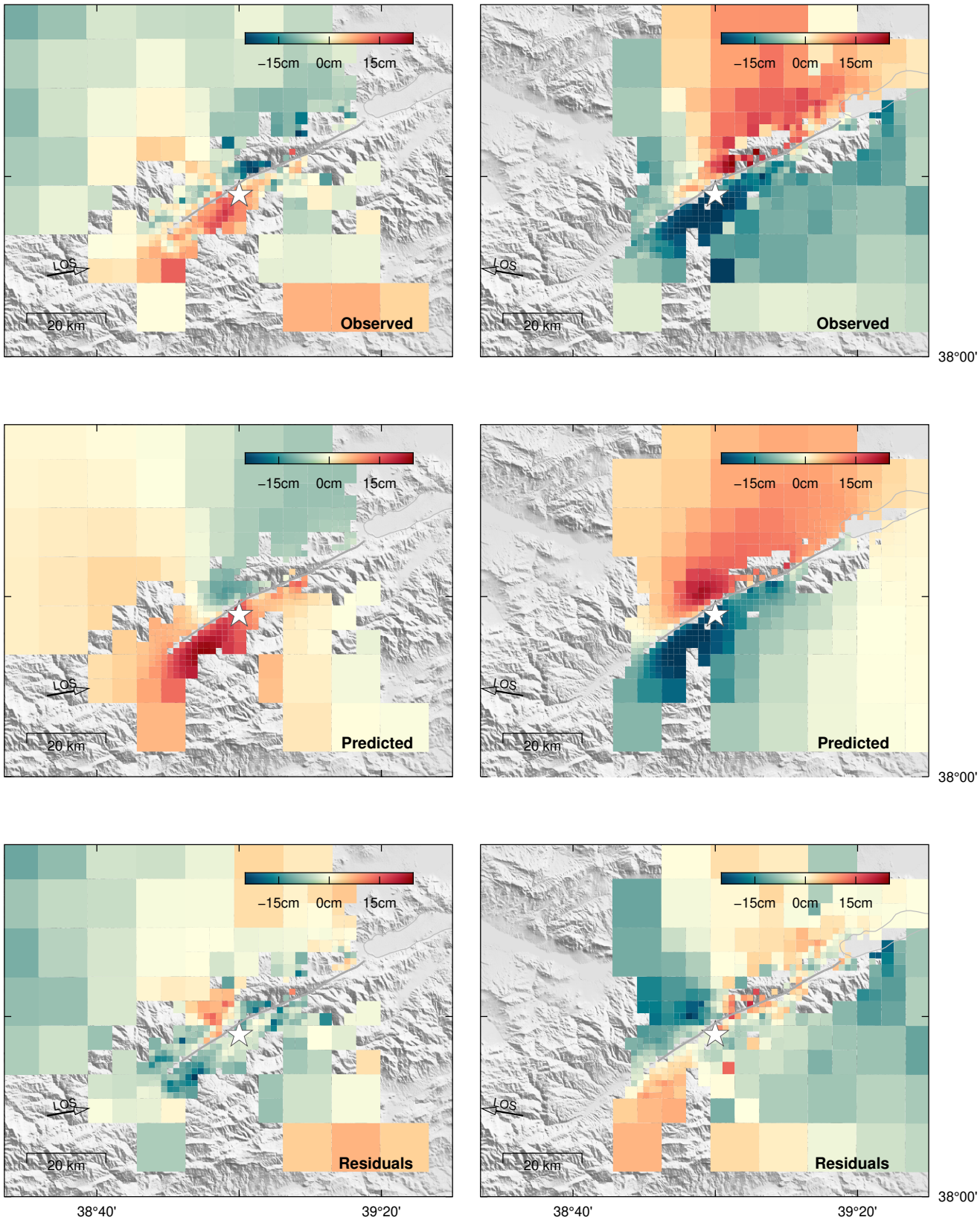

Figure S7. Observed and predicted pixel-offset surface displacement in the satellite azimuth direction for ALOS2 ascending (left) and descending (right) pairs. Predictions are inferred from the average model. The assumed fault trace is shown with a dark gray line.

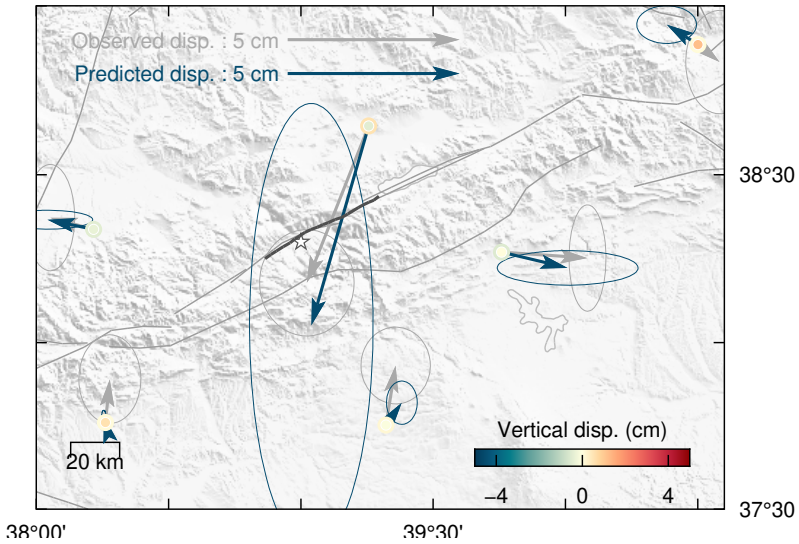

Figure S8. Observed and predicted surface displacement at the GNSS locations. Observed horizontal surface displacements are shown in gray with 90% confidence ellipses and vertical displacements as the inner amplitudes. Predicted horizontal displacements are shown in blue with 90% confidence ellipses and vertical displacements are the outer amplitudes. The assumed fault trace is shown with a dark gray line and the epicenter is the white star.

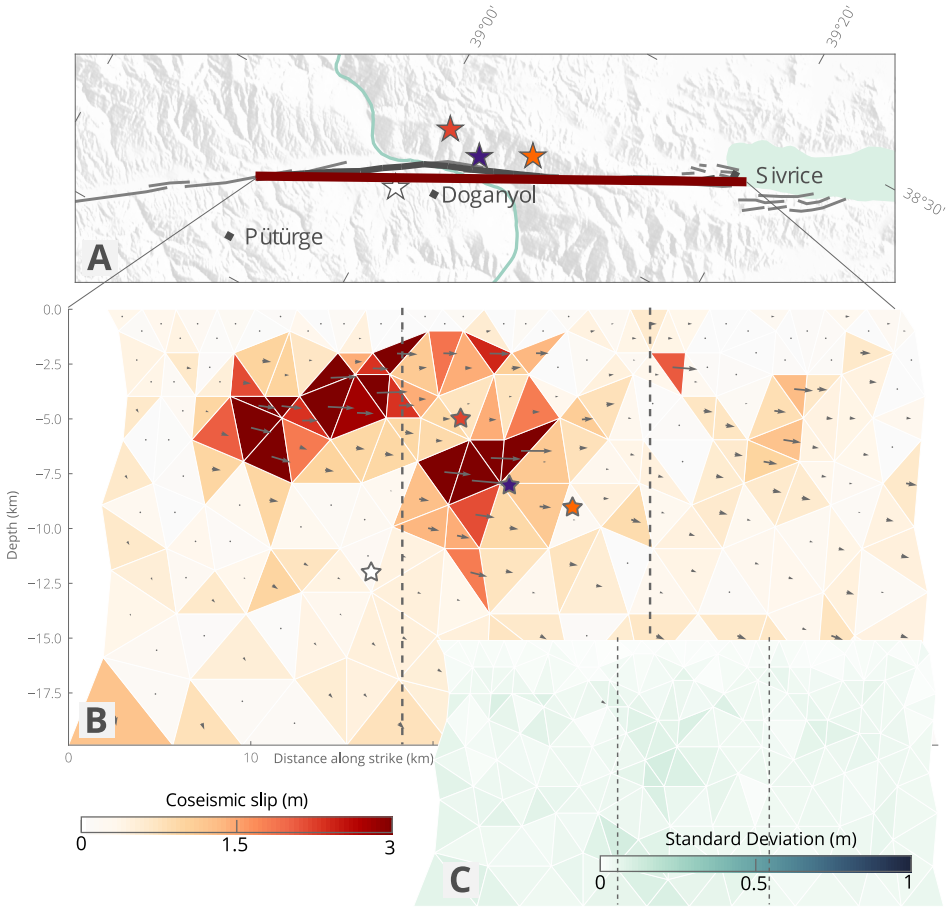

Figure S9. Inferred slip model and associated posterior uncertainty for the Elazığ earthquake, assuming a planar and vertical fault and no epistemic uncertainties. (a) Map view of the fault trace and local setting, possible epicenters are shown with white, red, purple and orange stars (from left to right on the map), respectively from GCMT, ? (?), KOERI and ? (?). (b) Depth view of the inferred total slip amplitudes and directions. (c) Standard deviation of the inferred strike-slip parameters.

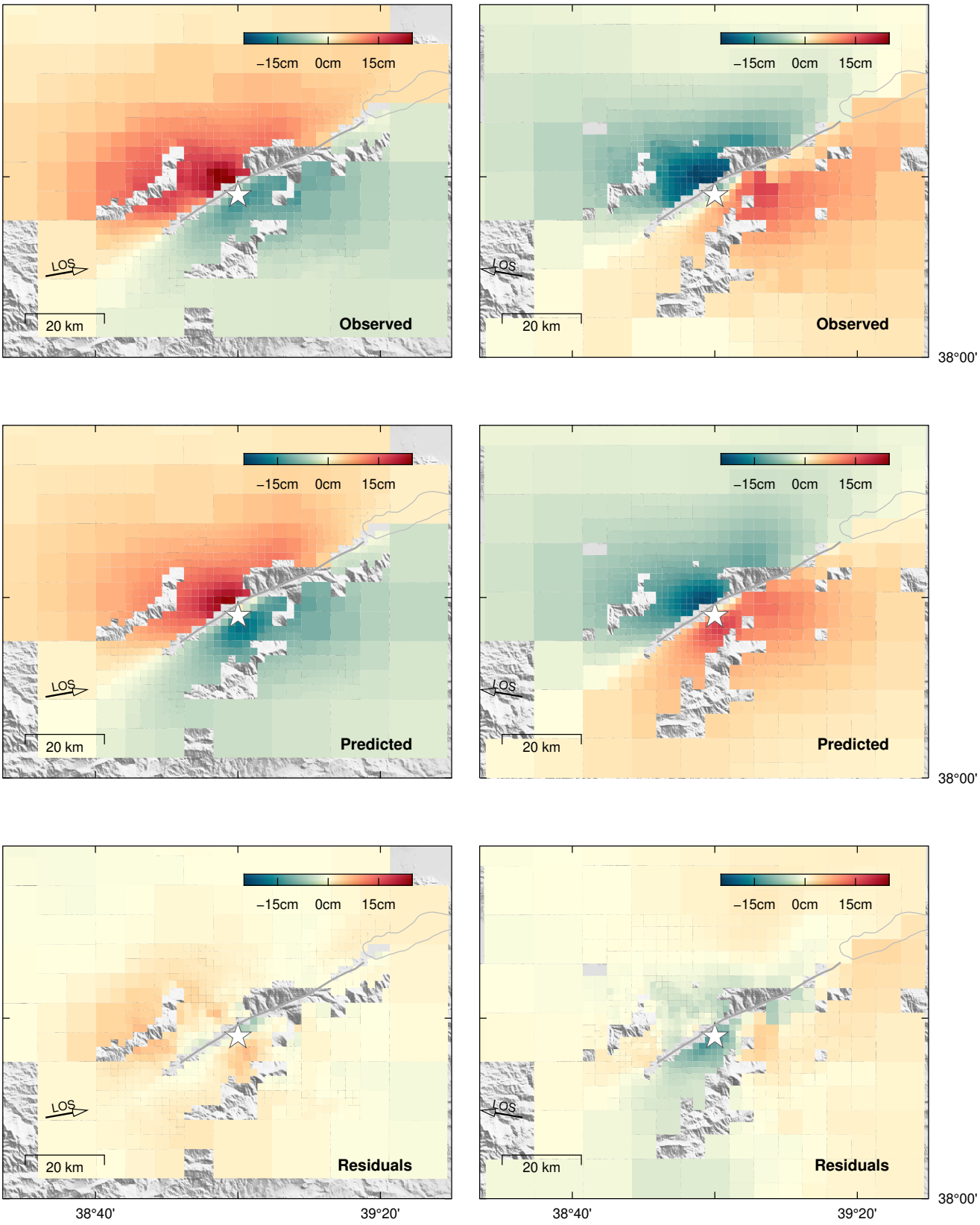

Figure S10. Observed and predicted surface displacement in the LOS direction for the Sentinel-1 ascending (left) and descending (right) interferograms. Predictions are inferred from the average model. The assumed fault trace is shown with a dark gray line.

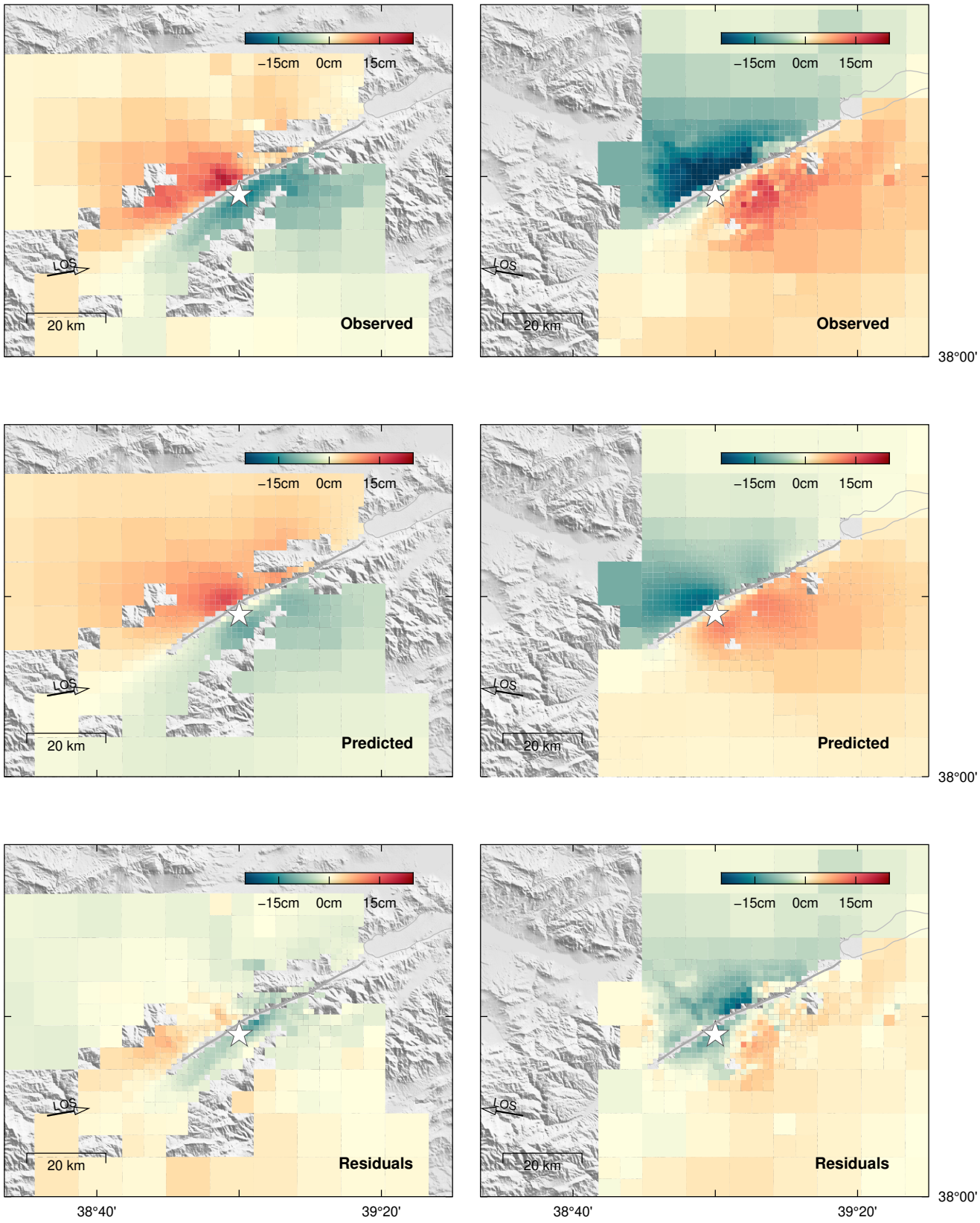

Figure S11. Observed and predicted surface displacement in the LOS direction for the ALOS 2 ascending (left) and descending (right) interferograms. Predictions are inferred from the average model. The assumed fault trace is shown with a dark gray line.

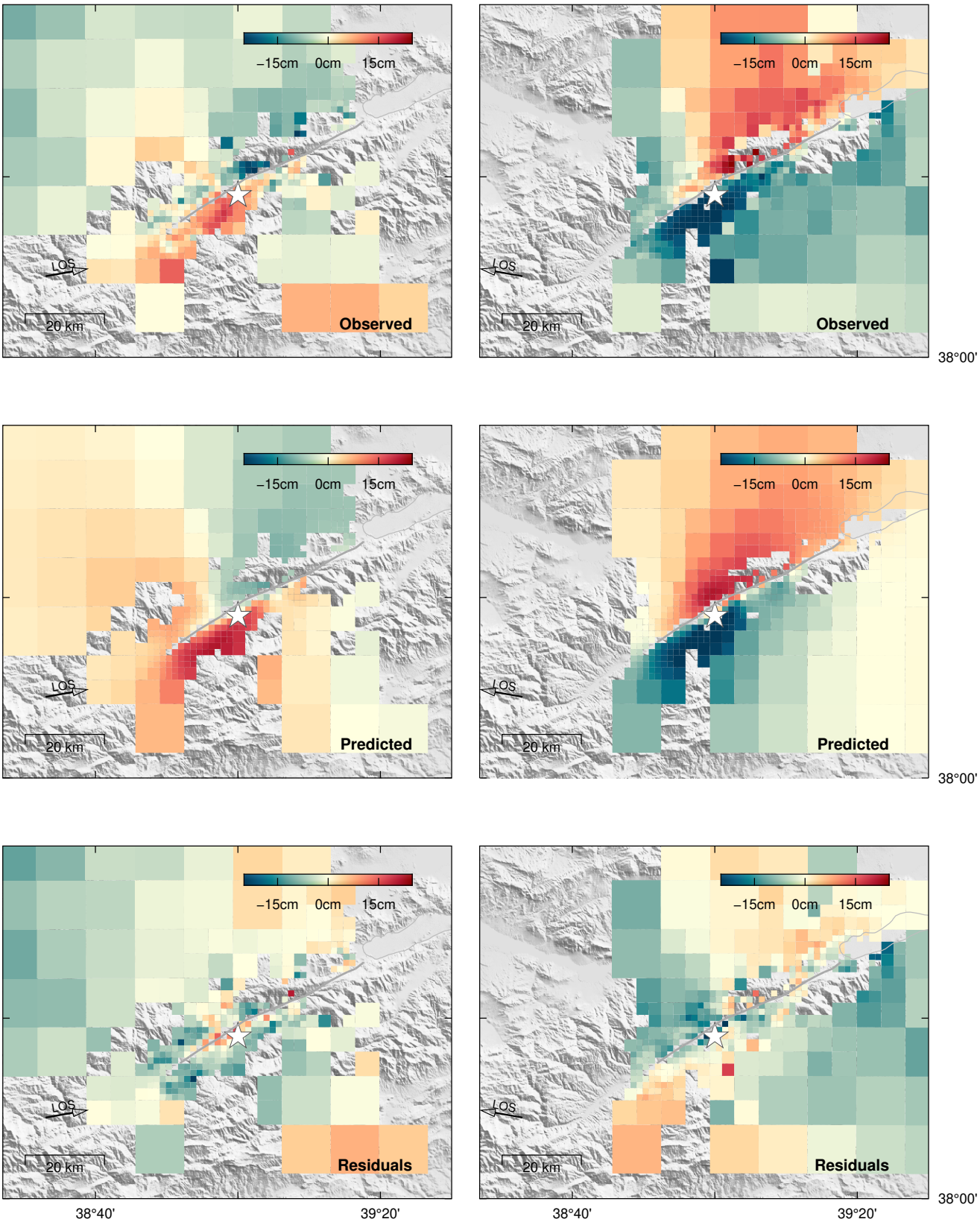

Figure S12. Observed and predicted pixel-offset surface displacement in the satellite azimuth direction for ALOS2 ascending (left) and descending (right) pairs. Predictions are inferred from the average model. The assumed fault trace is shown with a dark gray line.

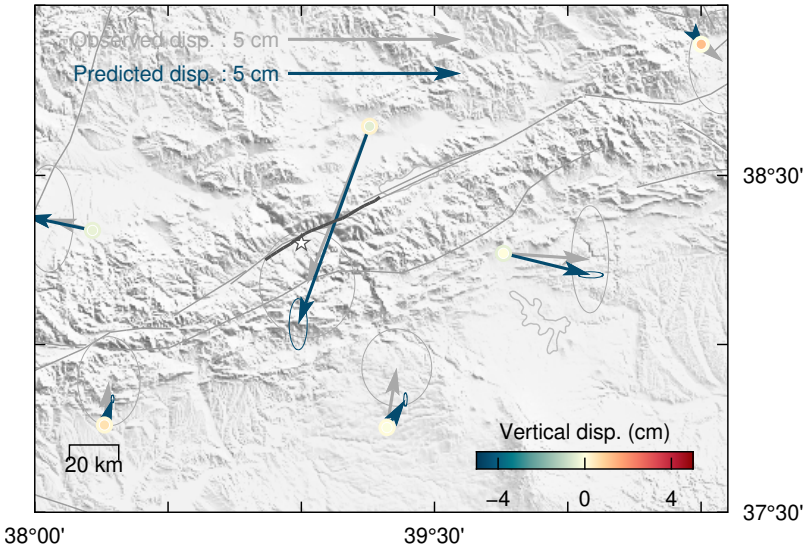

Figure S13. Observed and predicted surface displacement, assuming a planar fault, at the GNSS locations. Observed horizontal surface displacements are shown in gray with 90% confidence ellipses and vertical displacements as the inner amplitudes. Predicted horizontal displacements are shown in blue with 90% confidence ellipses and vertical displacements are the outer amplitudes. The assumed fault trace is shown with a dark gray line and the epicenter is the white star.

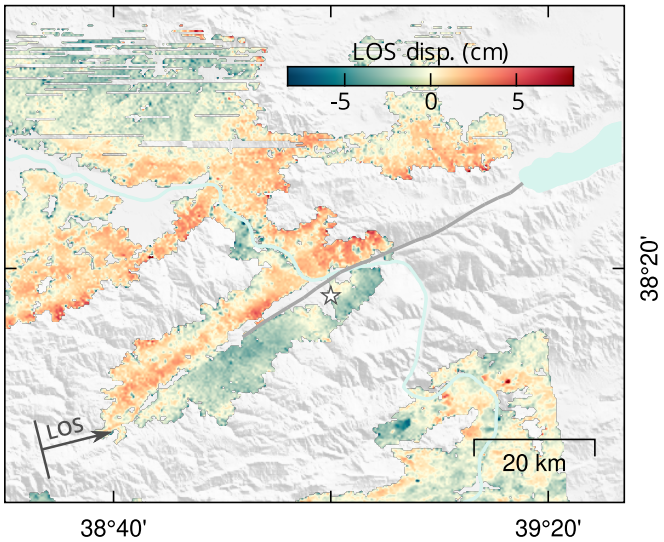

Figure S14. Surface displacement in the satellite line-of-sight (LOS) direction from an ALOS-2 ascending interferogram (01/31/2020-06/05/2020) covering 5 months of post-seismic deformation. The surface projection of the satellite LOS direction is positive in the ground-to-satellite direction.

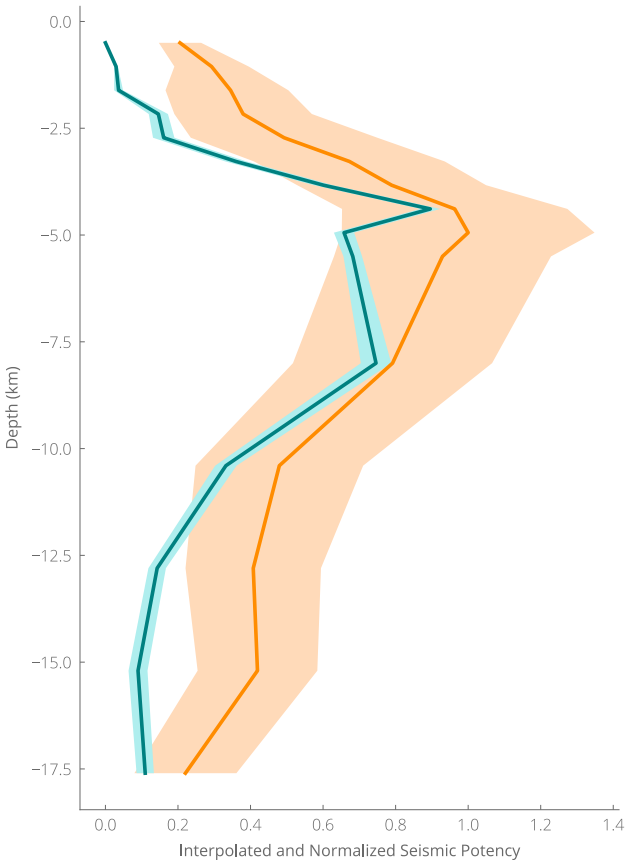

Figure S15. Seismic potency, interpolated and normalized by along-depth dimension and maximum potency, as a function of depth, for our preferred model accounting for uncertainties (orange) and our slip model neglecting epistemic uncertainties (blue). Standard deviation is shown with a lighter color. The seismic potency P_k for a particular depth range of index k is: $\mathrm{P}_k = \frac{\sum_i u_{ik}\ \mathrm{A}_{ik}}{d_k}$, u_{ik} being the slip interpolated for the considered portion of the fault, characterized by an along-depth width d_k and an area A_{ik}.

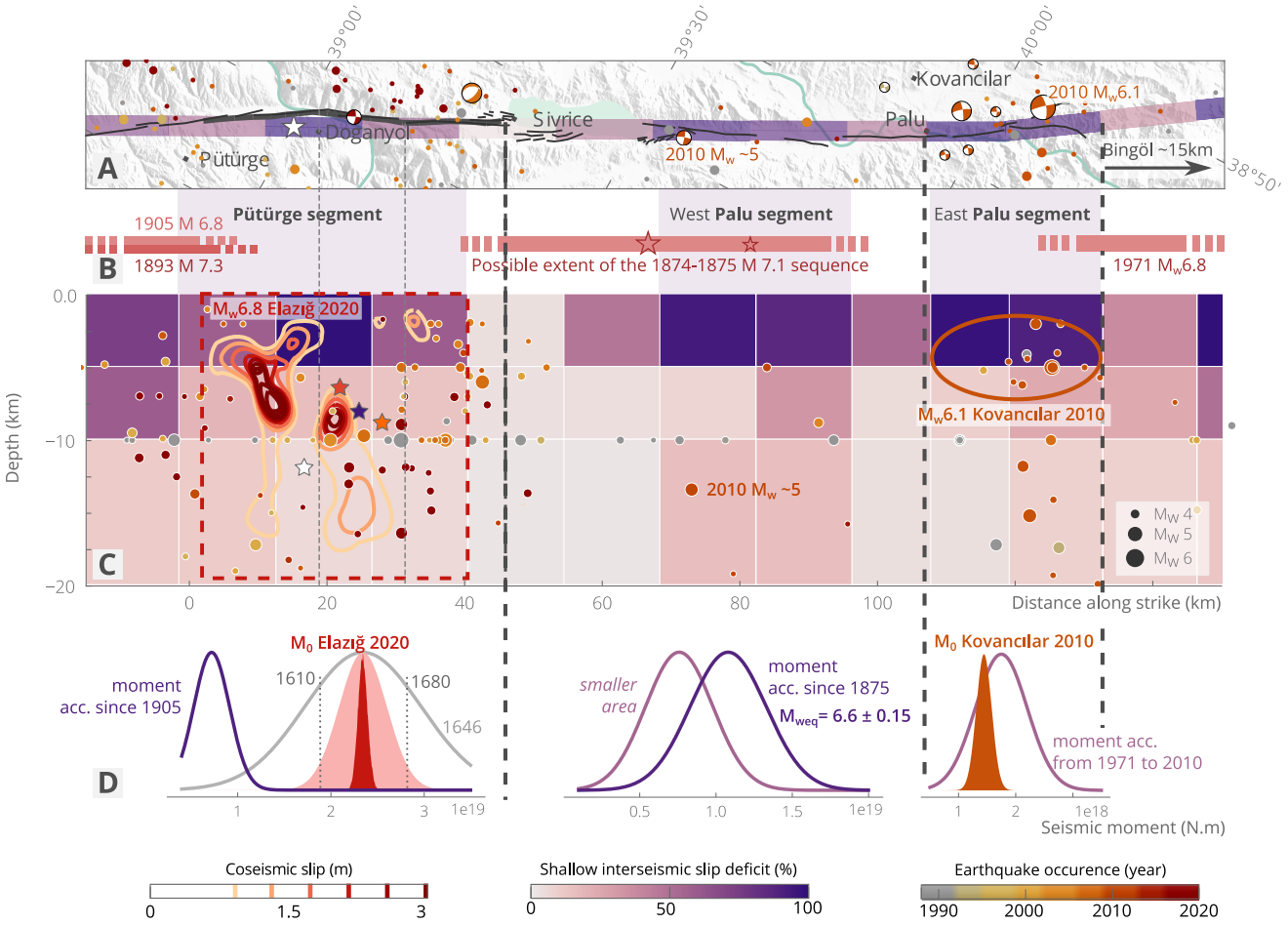

Figure S16. Same as Fig. 4 but in (c), the depth distribution of the interseismic slip deficit from Bletery et al. (2020).